

SANDIA REPORT

SAND2014-17359

Unlimited Release

Printed September 2014

Embedded Fiber Optic Sensors for Measuring Transient Detonation/Shock Behavior: Time-of-Arrival Detection and Waveform Determination

Marcus A. Chavez, Michael D. Willis, and Timothy T. Covert

Prepared by
Sandia National Laboratories
Albuquerque, New Mexico 87185 and Livermore, California 94550

Sandia National Laboratories is a multi-program laboratory managed and operated by Sandia Corporation, a wholly owned subsidiary of Lockheed Martin Corporation, for the U.S. Department of Energy's National Nuclear Security Administration under contract DE-AC04-94AL85000.

Approved for public release; further dissemination unlimited.



Sandia National Laboratories

Issued by Sandia National Laboratories, operated for the United States Department of Energy by Sandia Corporation.

NOTICE: This report was prepared as an account of work sponsored by an agency of the United States Government. Neither the United States Government, nor any agency thereof, nor any of their employees, nor any of their contractors, subcontractors, or their employees, make any warranty, express or implied, or assume any legal liability or responsibility for the accuracy, completeness, or usefulness of any information, apparatus, product, or process disclosed, or represent that its use would not infringe privately owned rights. Reference herein to any specific commercial product, process, or service by trade name, trademark, manufacturer, or otherwise, does not necessarily constitute or imply its endorsement, recommendation, or favoring by the United States Government, any agency thereof, or any of their contractors or subcontractors. The views and opinions expressed herein do not necessarily state or reflect those of the United States Government, any agency thereof, or any of their contractors.

Printed in the United States of America. This report has been reproduced directly from the best available copy.

Available to DOE and DOE contractors from

U.S. Department of Energy
Office of Scientific and Technical Information
P.O. Box 62
Oak Ridge, TN 37831

Telephone: (865) 576-8401
Facsimile: (865) 576-5728
E-Mail: reports@adonis.osti.gov
Online ordering: <http://www.osti.gov/bridge>

Available to the public from

U.S. Department of Commerce
National Technical Information Service
5285 Port Royal Rd.
Springfield, VA 22161

Telephone: (800) 553-6847
Facsimile: (703) 605-6900
E-Mail: orders@ntis.fedworld.gov
Online order: <http://www.ntis.gov/help/ordermethods.asp?loc=7-4-0#online>



Embedded Fiber Optic Sensors for Measuring Transient Detonation/Shock Behavior: Time-of-Arrival Detection and Waveform Determination

Marcus A. Chavez, Michael D. Willis, Timothy T. Covert

Energetic Materials Simulations and Fabrication (Organization 2556)
Sandia National Laboratories
P.O. Box 5800
Albuquerque, New Mexico 87185-MS1452

Abstract

The miniaturization of explosive components has driven the need for a corresponding miniaturization of the current diagnostic techniques available to measure the explosive phenomena. Laser interferometry and the use of spectrally coated optical windows have proven to be an essential interrogation technique to acquire particle velocity time history data in one-dimensional gas gun and relatively large-scale explosive experiments. A new diagnostic technique described herein allows for experimental measurement of apparent particle velocity time histories in microscale explosive configurations and can be applied to shocks/non-shocks in inert materials. The diagnostic, Embedded Fiber Optic Sensors (EFOS), has been tested in challenging microscopic experimental configurations that give confidence in the technique's ability to measure the apparent particle velocity time histories of an explosive with pressure outputs in the tenths of kilobars to several kilobars. Embedded Fiber Optic Sensors also allow for several measurements to be acquired in a single experiment because they are microscopic, thus reducing the number of experiments necessary. The future of EFOS technology will focus on further miniaturization, material selection appropriate for the operating pressure regime, and extensive hydrocode and optical analysis to transform apparent particle velocity time histories into true particle velocity time histories as well as the more meaningful pressure time histories.

ACKNOWLEDGMENTS

The authors would like to acknowledge the following individuals for helping to make EFOS a reality and push for a technical advance on the subject: John Liwski, Daniel Dow, Tom Pfeifle, and John Pavlakos. Without their comments, experimental aid, and dedication to this project, EFOS would be a relatively unknown and non-disseminated technology.

CONTENTS

1. Introduction.....	11
2. Laser Interferometer Description	15
2.1. Design and Construction.....	17
2.2. Mode of Detection	19
3. EFOS Experimental Measurements	21
4. EFOS Simulation Results.....	27
5. Conclusion.....	29
6. References	31

FIGURES

Figure 1-1 ^[6] , The expected cross-sectional view of the EFOS when over-sprayed by LIHE. The tips are as perpendicular to the surface to be sprayed and the elevation above this surface is precisely set and measured with an optical comparator to within $\pm 2 \mu\text{m}$. The fibers feed back into the PDV laser system. Note that the diagnostic does not need to be embedded in reacting explosives, but can also detect compression waves of shock and non-shock nature through inert materials.....	12
Figure 1-2 ^[6] , Left photo is the final assembly of a fiber rosette ready to be installed into a target. The four fibers protrude out of four closely spaced 17 mil diameter drilled holes. Right photo shows the same fiber rosette under an optical comparator with the longest fiber in focus. Note that the right image has a scale bar that correlates only to the shadow graphs produced with an optical comparator.	12
Figure 1-3, Left is a three-dimensional CAD model showing the typical parts of an EFOS. Right CAD model shows the EFOS in a close-up view, offering more details about the device. A detail of the geometry and associated dimensions gives an idea of the size of the probe.	13
Figure 1-4, Left CAD model shows a close-up view of the assembled rosette that was built to specifications as shown in Figure 1-2. Right CAD model allows for a see-through view that illustrates EFOS as they were employed in experiments with SASN explosive spray deposited over the top of the probe tips.	13
Figure 1-5, Image is zoomed out from previous figure and allows for comparison to the photo on the left in Figure 1-2.	14
Figure 2-1, The LIHE Facility acoustic-optical up-shifted PDV system running with a beat frequency signal of 500 MHz ^[11]	16
Figure 2-2, Snapshot of the LIHE's PDV internal components, which is closely related to the previous figure's detailed description.....	17
Figure 2-3, Left illustration shows detail of the EFOS fiber tip. The right image displays the spectral coating material types, thicknesses, and order of deposition.	18
Figure 2-4, Top view of EFOS Rosette, in Cartesian coordinates from test TP49. Fiber tip center locations are marked by blue diamonds and the approximate fiber tip diameters are the black circles surrounding the blue diamonds. This shows the distances and locations each EFOS probe is from one another and is typical for all EFOS in rosettes presented here. Future diagnostics, such as surface profilometers, may be able to capture the topography generated from the fibers to	

and allow direct export of three-dimensional fiber arrangements into hydrocodes for model validation.	18
Figure 2-5, Illustration A shows the unreacted porous LIHE subjected to irradiation with subsequent initiation points in illustration B after some induction time. Illustration C is some time after illustration B in which the original initiation points expand in a spherical fashion towards one another to coalesce, leaving reaction products in the centers. The extent of reaction is represented by the color, with red being less reacted and progressing to yellow being fully reacted. Much of the coalescing is done in a regressive fashion. Illustration D shows a cohesive reaction wave that is composed of wavelets that vary spatially at any given time, usually dampening to a quasi-planar wave front.	19
Figure 3-1 ^[6] , Apparent particle velocity traces from EFOS in the unaltered SASN explosive assumed to be ignited from the exposed outer surface by high intensity visible and ultraviolet light.	22
Figure 3-2 ^[6] , Apparent particle velocity traces from EFOS in the 4% Triton X-100/SASN explosive ignited from the exposed outer surface by high intensity visible and ultraviolet light. Notice the PDV6 trace has a negative particle velocity for the suspected surface reflection timing fiducial.	22
Figure 3-3 ^[6] , Apparent particle velocity traces from EFOS in the 5% Viton B600/SASN explosive ignited from the exposed outer surface by high intensity visible and ultraviolet light. Notice traces PDV 7 (green) and PDV6 (tan) are missing the distinguishable and suspected surface reflection timing fiducials. Notice the inverted suspected surface reflection timing fiducial for the trace of EFO5 (red).	23
Figure 3-4 ^[6] , XT plot for the EFOS from each explosive mix tested in TP49 giving the first true reaction wave velocities through the thickness of thin spray-deposited explosive when the exposed outer surface is light initiated. The slope of each line is the average wave front velocity for that particular explosive. The wave front velocity is most likely a deflagration velocity. Error bars are deduced from the adjacent coupon thickness measurements.	23
Figure 3-5, Apparent particle velocity traces from EFOS in the pure SASN. The surface reflect shock timing fiducial is arrives after the wave front of EFO5, but smaller amplitude fiducials also appear in the other traces around the same time.	24
Figure 3-6, Apparent particle velocity waveforms from EFOS in Viton B600 doped SASN explosive. These traces were exceptionally noise-less and gave clear timing for determination of the reaction front velocity. The large amplitude reflected shock timing fiducial appears in the apparent particle velocity trace, EFOS6.	24
Figure 3-7, Apparent particle velocity time histories for the high bulk density Viton doped SASN explosive. The ignition delay was longer and the traces all nearly overlap for the first 35 μ s, except EFO5. The Viton doped SASN had the tendency to cover the fibers even though they were above the average thickness of the explosive, thus recording similar apparent particle velocity traces. This is an indication of the fiber diameters obstructing the measurement. Video of the explosive during spray deposition showed the protrusion of the fibers under the explosive surface, much like snow covering rocks.	25
Figure 3-8, XT diagram of the EFOS from two explosive mixes tested in TP51 allowing for reaction wave velocity determination through the thickness of thin spray-deposited explosive when the exposed outer surface is light initiated. The slope of each line is the average wave front velocity for that particular explosive. The wave front velocity is most likely a deflagration velocity. Error bars are deduced from the adjacent coupon thickness measurements.	25

Figure 4-1 ^[6] , Two-dimensional CTH modeling results for arbitrary SASN detonation wave impacting one EFOS tip and reflecting off the aluminum substrate. This is the particle velocity in the fiber that the EFOS would see if corrected for the index of refraction as well as the shock-induced change in the index of refraction. However, rarefaction effects are still evident and need to be corrected for in order to produce the true particle velocity of the fiber tip.	27
Figure 4-2, Stress time history corresponding to the same tracer locations from Figure 17 above. The second major particle velocity jump has a complementary stress. This reflected stress emanated from an input stress that is the deflagration/detonation wave. Thus, through proper transformations, the EFOS could reveal the pressure time history of an energetic material at that location in the flow.	28
Figure 4-3 ^[6] , Image from two-dimensional CTH simulation of two EFOS in a typical experimental geometry seen in TP49. The tallest EFOS is at an elevation of 254 μm and the shorter one is at 127 μm . The white and gray colored areas in the model are particle velocities that are above the upper color map range.	28

NOMENCLATURE

Acronyms

BUD	Build-up of detonation
CAD	Computer aided design
CTH	Cubit to the three halves, a hydrocode program
DDT	Deflagration-to-detonation transition
DOD	Department of Defense
DOE	Department of Energy
EFOS	Embedded fiber optic sensors
LIHE	Light initiated high explosive
PDV	Photonic Doppler velocimetry
SASN	Silver acetylide-silver nitrate explosive
SIRHEN	Sandia infrared heterodyne analysis program
SMF	Single Mode Fiber
SNL	Sandia National Laboratories
PMMA	Polymethyl methacrylate
TOA	Time-of-arrival
TOAD	Time-of-arrival detector or device
TP	Test plan
XT	Distance-time
VISAR	Velocity interferometer system for any reflector

Units

Time

<i>s</i>	Seconds
μs	Microseconds

Distance, Length, or Thickness

\AA	Angstroms
<i>nm</i>	Nanometers
μm	Micrometers or microns
<i>mm</i>	Millimeters
<i>mil</i>	Thousandth of an inch (1 mil=25.4 μm)

Velocity

<i>mm/μs</i>	Millimeters/microsecond
<i>cm/s</i>	Centimeters/second
<i>m/s</i>	Meters/second

Density

<i>mg/cm²</i>	Milligrams/centimeter ²
<i>g/cm³</i>	Grams/centimeter ³

Pressure or Stress

<i>dyne/cm²</i>	Dyne/centimeter ² , 10 ⁹ dyne/cm ² =1 kbar
----------------------------	---

kbar Kilobar

Frequency

MHz Mega Hertz (10^6 cycles/s)

GHz Giga Hertz (10^9 cycles/s)

Power

mW Milliwatts

Non-dimensional

m/m Mass/mass, can be in a percentage, %

Variables

P_{spike} Pressure spike of an explosive, i.e. can be von Neumann or Chapman-Jouguet spike measured in kbars

ρ_{AD} Areal density of SASN LIHE measured in mg/cm^2

λ Wavelength measured in nm

\emptyset Diameter measured in μm

1. INTRODUCTION

Energetic materials research has led to an increased interest with miniaturization of energetic based components to the microscale. This has paved a path for probing fundamental behavior that occurs in explosives on the microscale. Running parallel in the same realm, interest in dynamic pressure loading of inert materials has become increasingly important. Diagnostics that measure these events are relatively large by comparison and generally do not allow unobtrusive interrogation of the physical phenomena of interest in microscopic components or experimental configurations. Conventionally, laser interferometry is paired with spectrally coated optical windows which are subjected to a dynamic pressure load, sometimes a non-shock or shock event, and measure the apparent particle velocity induced into the window material ^[1]. The scale of the experiment is typically measured on the order of millimeters or larger for the distance which the dynamic pressure loading, or stress, has to traverse. The lateral dimensions for such experiments are on the order of centimeters to achieve one-dimensional loading conditions.

A developed and recently implemented diagnostic at the Light Initiated High Explosives (LIHE) facility utilizes a laser interferometry system, called photonic Doppler velocimetry (PDV), which is coupled with fiber optic sensors to measure transient explosive and shock/non-shock behavior. Typical names for explosive transient behavior are deflagration-to-detonation transition (DDT) and build-up of detonation (BUD). This system was used to measure apparent particle velocity at several locations in light sensitive explosives based on the primary explosive called silver acetylide-silver nitrate (SASN). The detonation velocity of SASN based explosives have been historically measured in the same manner as other explosives; with a relatively long strip of the explosive initiated on one end and time-of-arrival (TOA) pins at known distances, usually in inches, from the ignition point ^[2-5]. Typical measurements ranged from 0.5 to 1.5 mm/ μ s for areal densities (ρ_{AD}) of SASN explosive ranging from 11.4 to 118.8 mg/cm² ^[2-5] as measured historically and in recent experiments at the LIHE facility. This type of measurement does well for determining steady-state sweeping waves, but neglects the nearly one-dimensional unsteady wave propagation a LIHE can offer on the order of hundreds of microns or less since an LIHE ignites from the exposed outer surface and burns towards the substrate it is spray-deposited onto. This particular experimental challenge led to the development of Embedded Fiber Optic Sensors (EFOS) to measure apparent particle velocity and deduce TOA at several locations normal to the reactive wave front on the microscale. Context on the SASN explosive its use, and the can be found in references 2-6.

The first test of the EFOS diagnostic was in the LIHE experiment TP48 (Test Plan). The outcome of that test series determined the most efficient means of measuring transient explosive response. The best orientation of the fiber tip is to be perpendicular to the incoming deflagration, detonation, or shock wave as shown in Figure 1-1. This is due to the reflection of the reactive wave front with the fiber tip is maximized in this orientation. In order to effectively measure the deflagration/detonation velocity of SASN based LIHEs, four fibers were placed adjacent one another in a rosette arrangement at several positions along the reactive wave front propagation axis. The LIHE facility can embed up to eight of these probes in a single experiment with the current PDV system. The illustrations and photographs in Figure 1-1 through Figure 1-5 shows the diagnostic as it was employed in test series TP49 and TP51.

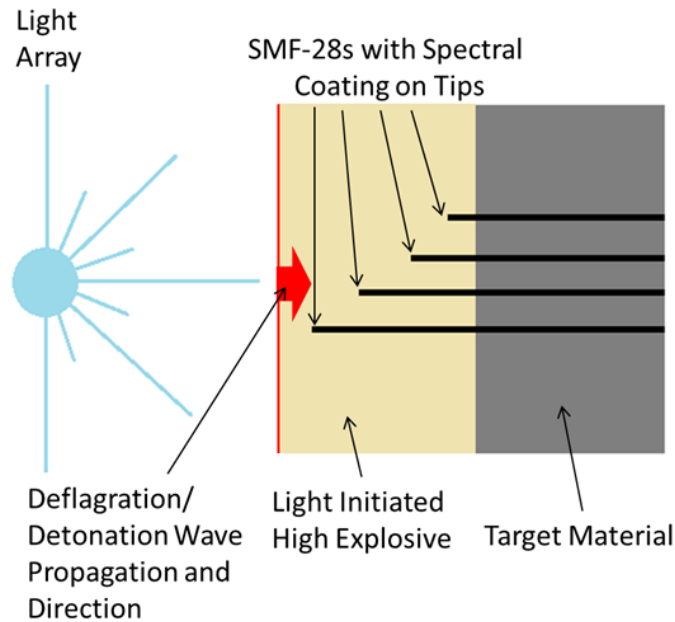


Figure 1-1^[6], The expected cross-sectional view of the EFOS when over-sprayed by LIHE. The tips are as perpendicular to the surface to be sprayed and the elevation above this surface is precisely set and measured with an optical comparator to within $\pm 2 \mu\text{m}$. The fibers feed back into the PDV laser system. Note that the diagnostic does not need to be embedded in reacting explosives, but can also detect compression waves of shock and non-shock nature through inert materials.

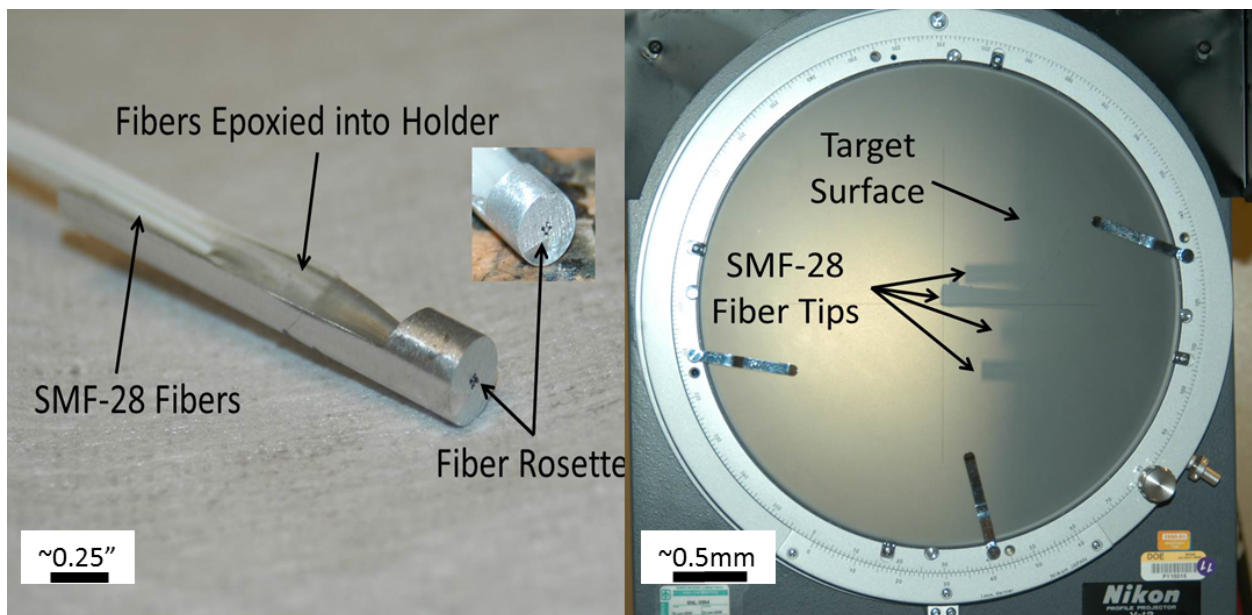


Figure 1-2^[6], Left photo is the final assembly of a fiber rosette ready to be installed into a target. The four fibers protrude out of four closely spaced 17 mil diameter drilled holes. Right photo shows the same fiber rosette under an optical comparator with the longest fiber in focus. Note that the right image has a scale bar that correlates only to the shadow graphs produced with an optical comparator.

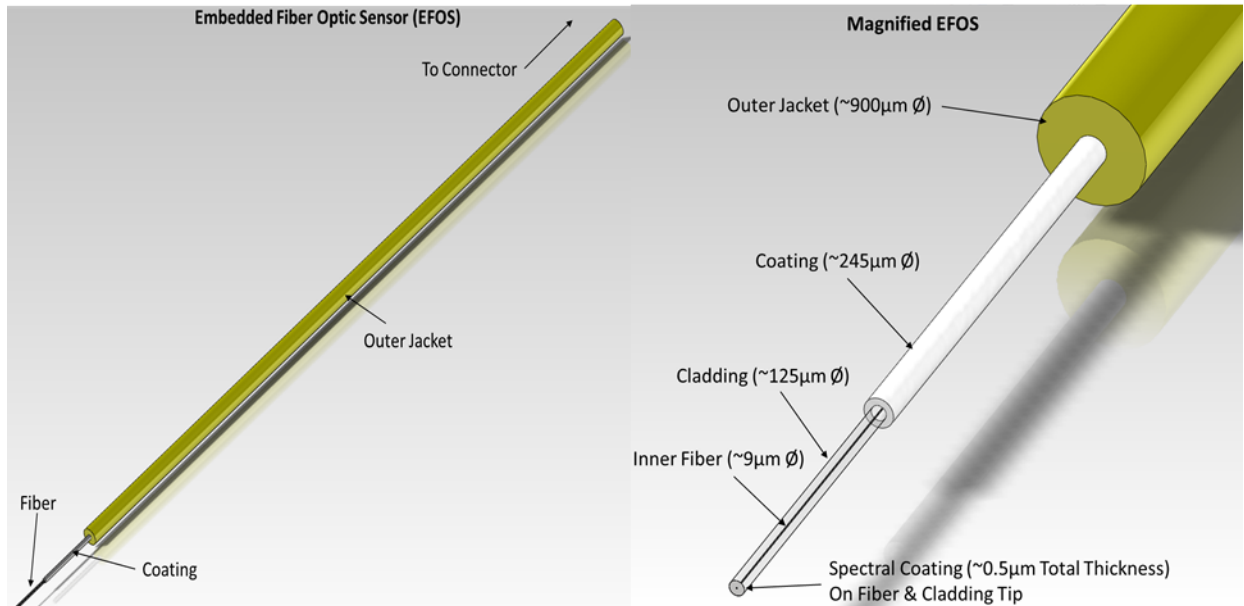


Figure 1-3, Left is a three-dimensional CAD model showing the typical parts of an EFOS. Right CAD model shows the EFOS in a close-up view, offering more details about the device. A detail of the geometry and associated dimensions gives an idea of the size of the probe.

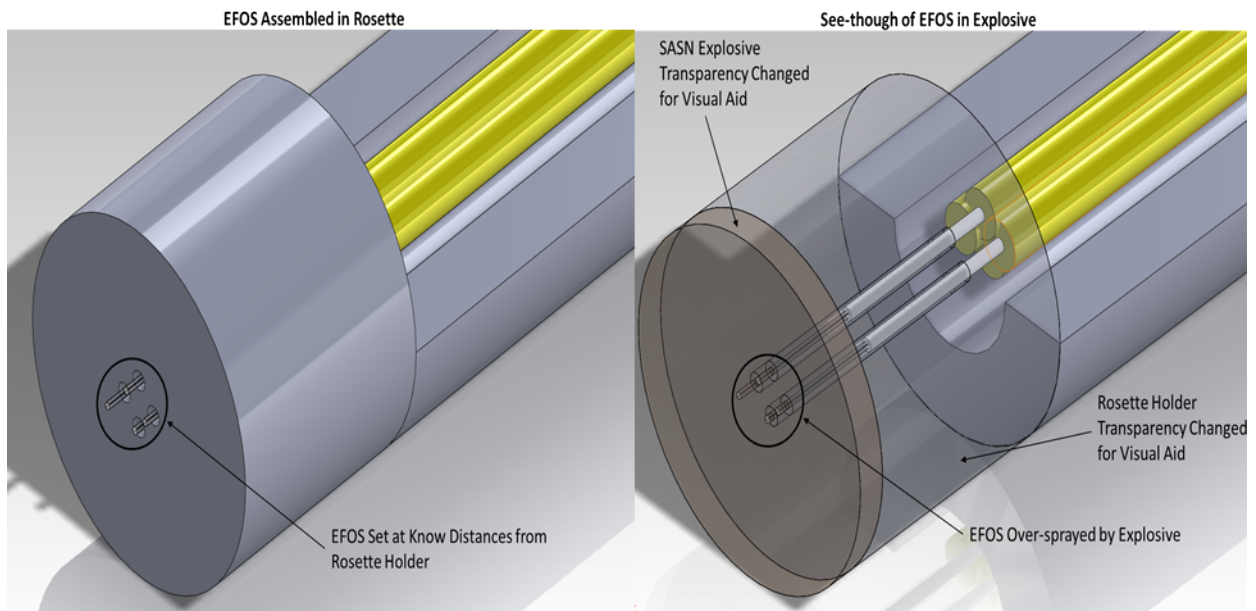


Figure 1-4, Left CAD model shows a close-up view of the assembled rosette that was built to specifications as shown in Figure 1-2. Right CAD model allows for a see-through view that illustrates EFOS as they were employed in experiments with SASN explosive spray deposited over the top of the probe tips.

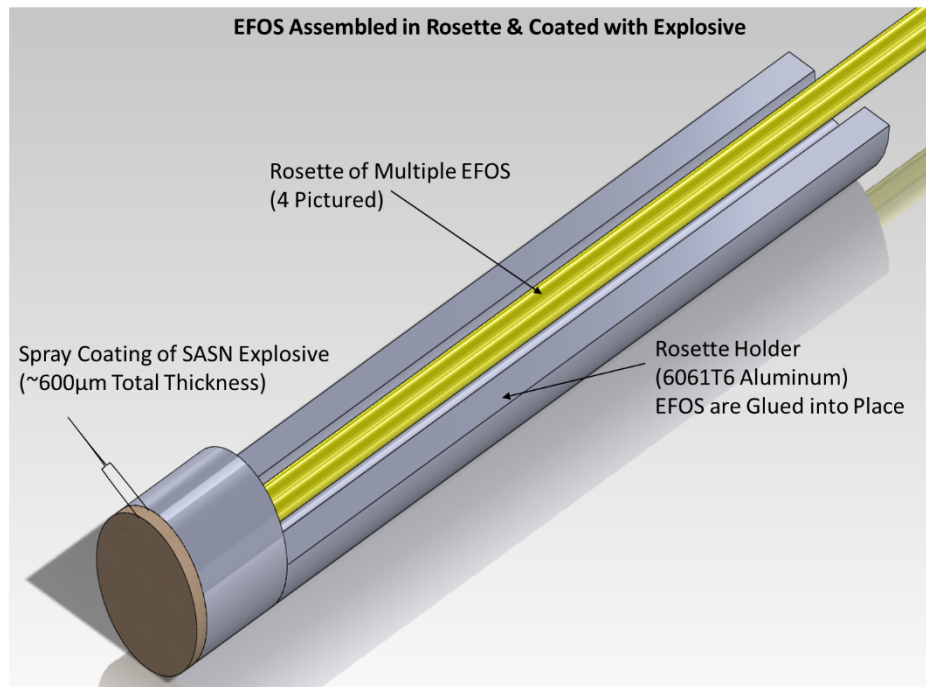


Figure 1-5, Image is zoomed out from previous figure and allows for comparison to the photo on the left in Figure 1-2.

2. LASER INTERFEROMETER DESCRIPTION

The laser interferometer, PDV, uses the Doppler shifted light reflected from a moving source (spectral or diffuse reflective surface) combined with non-Doppler shifted light from a stationary reference to create an interference or beat frequency^[7-10]. The velocity, such as the particle velocity of the reflective surface, is proportional to the beat frequency. By using a reference light source with a different frequency than the measurement light source, a beat frequency is created with a non-moving reflective surface yielding diagnostic advances. This “up-shifted” technique is achieved either through the use of a Bragg crystal acousto-optic amplifier or a tunable laser. The sensitivity for the detectable amount of displacement is half the wavelength of the laser source for a minimum time that the detector and digitizer can detect with a sufficiently large signal to noise ratio^[10].

The LIHE Facility PDV system uses a 1550 nm wavelength infrared laser, which can detect 775 nm of normal displacement (assuming no change in index of refraction) from a spectral surface^[8-10]. An apparent change in the spectral surface’s position can be produced by a change in the index of refraction of the medium the laser light is traveling through. This can result in the optical path length change of 775 nm, but this is only an apparent change and not the actual length of the medium. The optical effects stem from mechanical and thermal inputs into the fiber system. Bending the fibers produces an apparent particle velocity shift as does thermal expansion or contraction of the fiber. Thus the EFOS can be utilized for different environments than the current study demonstrates.

The infrared detectors have a 2 GHz bandwidth and the digitizers were of 2.5 GHz bandwidth. An “up-shifted” PDV system using a fixed acousto-optic amplifier at 500 MHz has a working range of measurable velocities from less than 0.01 m/s to 387.5 m/s as long as the signal to noise ratio is greater than one, especially in the low velocity regime^[8,10]. Greater velocity ranges may be achieved with a higher frequency acousto-optic amplifier or using a tunable laser for the reference source. The LIHE Facility’s PDV system and all the inner workings are presented in Figure 2-1 and Figure 2-2. Additionally to note, the power output near the fiber tip is on the order of 10-50 mW and was not able to ignite the sensitive primary explosive prior to the ignition source functioning. The power output at the tip is dependent on bending of the fibers, coating quality, laser interferometer output, etc.^[10].

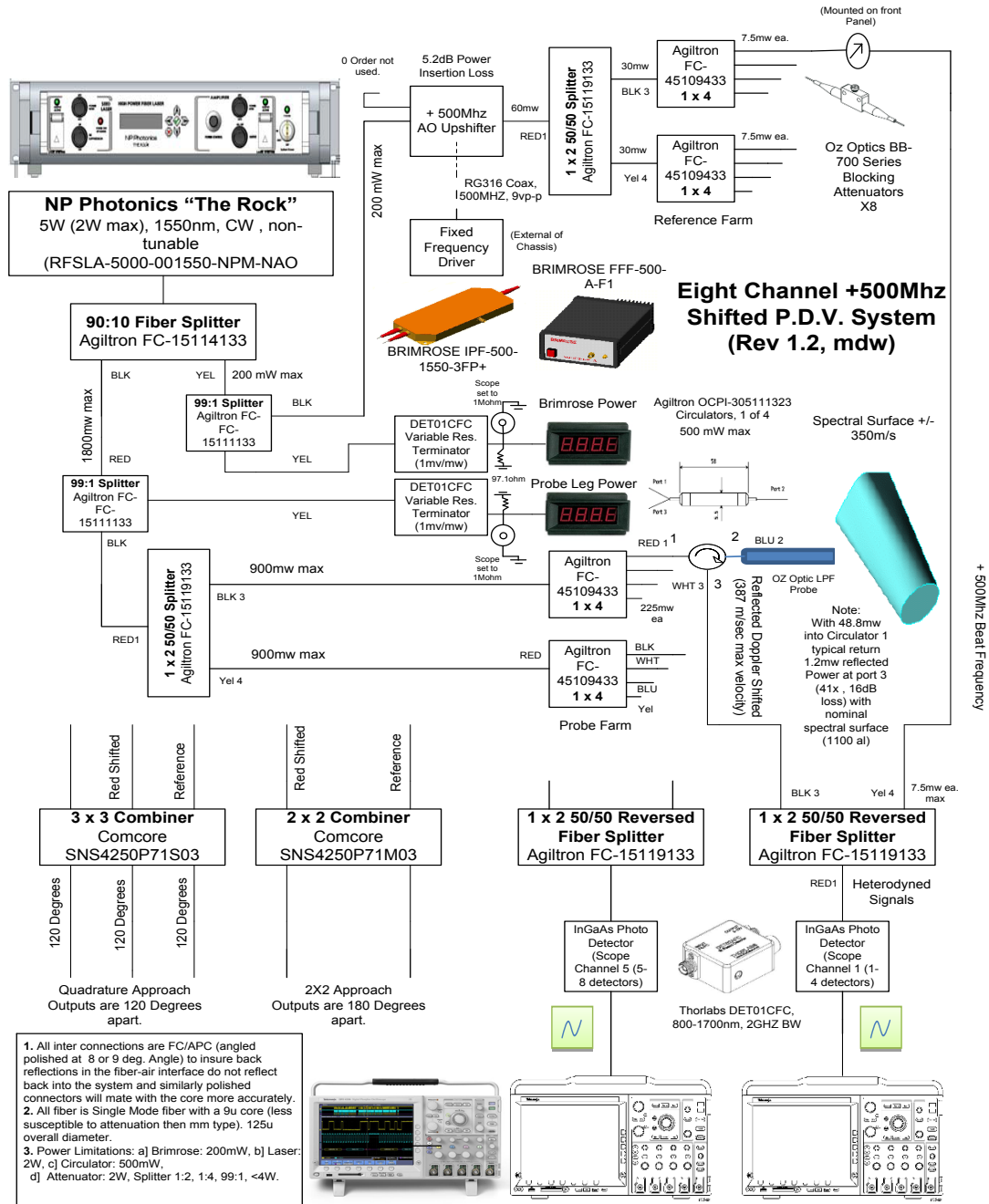


Figure 2-1, The LIHE Facility acoustic-optical up-shifted PDV system running with a beat frequency signal of 500 MHz [11].

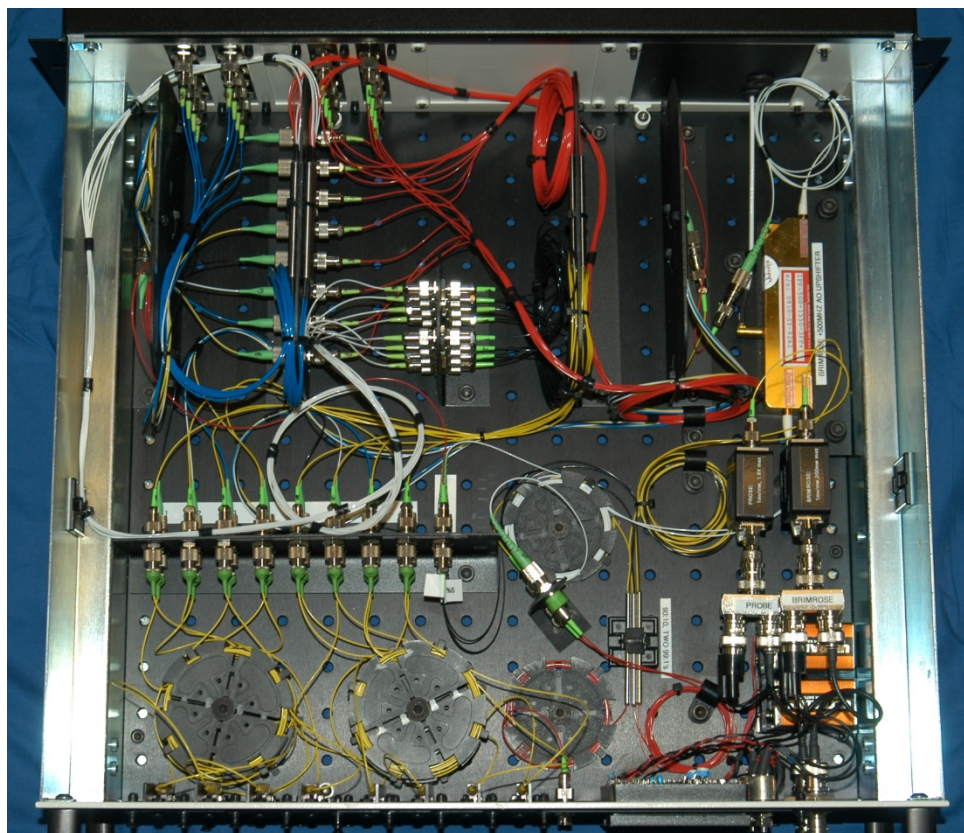


Figure 2-2, Snapshot of the LIHE's PDV internal components, which is closely related to the previous figure's detailed description.

2.1. Design and Construction

The original EFOS were manufactured using plane-cleaved Corning SMF-28 9/125 μm diameter fibers. A coating of 4000 \AA aluminum was physically vapor deposited to achieve the spectral coating of on the plane-cleaved tip. More advanced EFOS had a coating of 3500 \AA thick aluminum spectral surface over a 500 \AA titanium layer for adherence to the fiber tip. Over the aluminum was a 1000 \AA layer of aluminum oxide to act as a protective coating as seen in Figure 2-3. This is the preferred arrangement for EFOS because of the robustness of the coating. A 25.4 mm segment of fiber jacket was cut away to expose the coated fiber tip for use in this study's experiments. The completed fibers are then installed very carefully into the EFOS probe holder with an optical comparator and laser alignment tools to precisely achieve the desired locations. The accuracy of using the optical comparator is on the order of $\pm 2 \mu\text{m}$. Better diagnostics could be used to position the fibers in future experiments as well as capture the distance between fiber tips. Figure 2-4 shows a typical EFOS probe tip location from a top view and illustrating the current ability to locate EFOS relative to one another in the X-Y axes. The actual fiber optic is composed of fused silica batched and drawn at DuPont with a 9 μm inner core diameter and outer core diameter measured at the LIHE facility to range from 121 to 130 μm . Since the fiber diameter has some amount of range associated with it, it is prudent to measure the diameter to ensure proper accounting for refraction effects in the future.

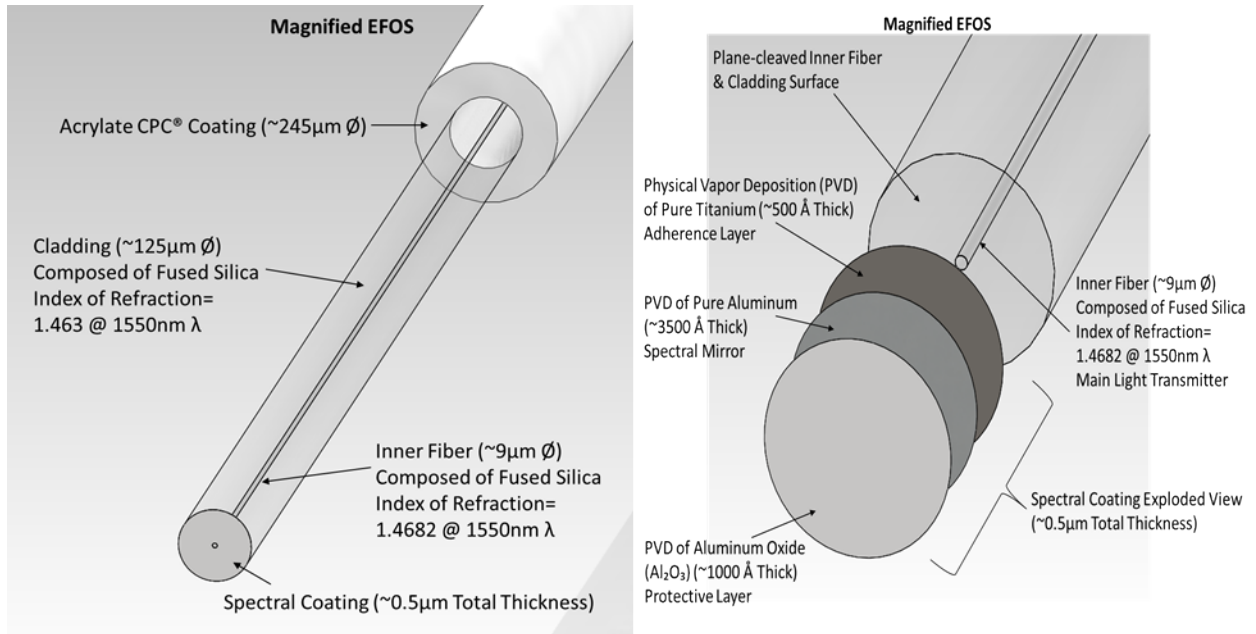


Figure 2-3, Left illustration shows detail of the EFOS fiber tip. The right image displays the spectral coating material types, thicknesses, and order of deposition.

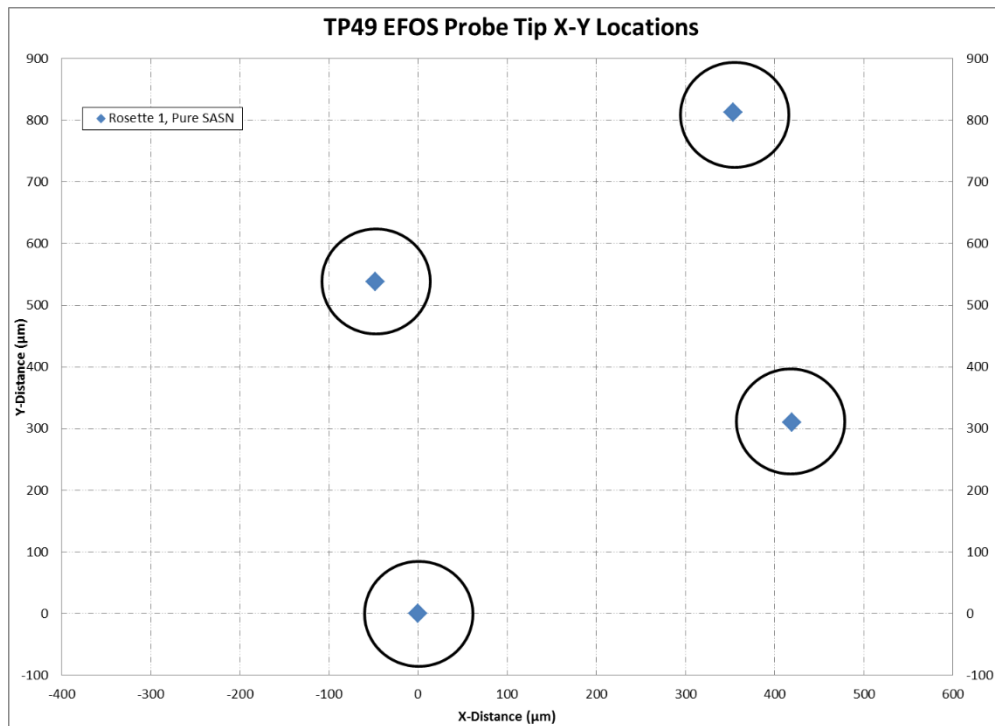


Figure 2-4, Top view of EFOS Rosette, in Cartesian coordinates from test TP49. Fiber tip center locations are marked by blue diamonds and the approximate fiber tip diameters are the black circles surrounding the blue diamonds. This shows the distances and locations each EFOS probe is from one another and is typical for all EFOS in rosettes presented here. Future diagnostics, such as surface profilometers, may be able to capture the topography generated from the fibers to and allow direct export of three-dimensional fiber arrangements into hydrocodes for model validation.

2.2. Mode of Detection

The original idea was to introduce relatively non-invasive time-of-arrival devices (TOADs) to measure the actual deflagration and/or detonation velocity produced by light initiated SASN explosive at several locations within the reaction flow. The fibers needed to be placed in close proximity to each other no longer than the total thickness of the explosive coating to avoid multi-dimensional reactive wave fronts. The reasoning behind this rule of thumb is as follows; ignition occurs at many points near the exposed surface that eventually coalesce into a cohesive reaction front some distance into the unreacted explosive. Figure 2-5 attempts to describe, step-by-step, the issue with using a single probing point in a real explosive upon ignition. Since the LIHE type of experiment is only quasi-one-dimensional, the interpretation of data becomes difficult with single probing points along the flow. Thus larger arrays with multiple probes at each depth within the explosive would be more representative of the non-steady reaction wave front propagation.

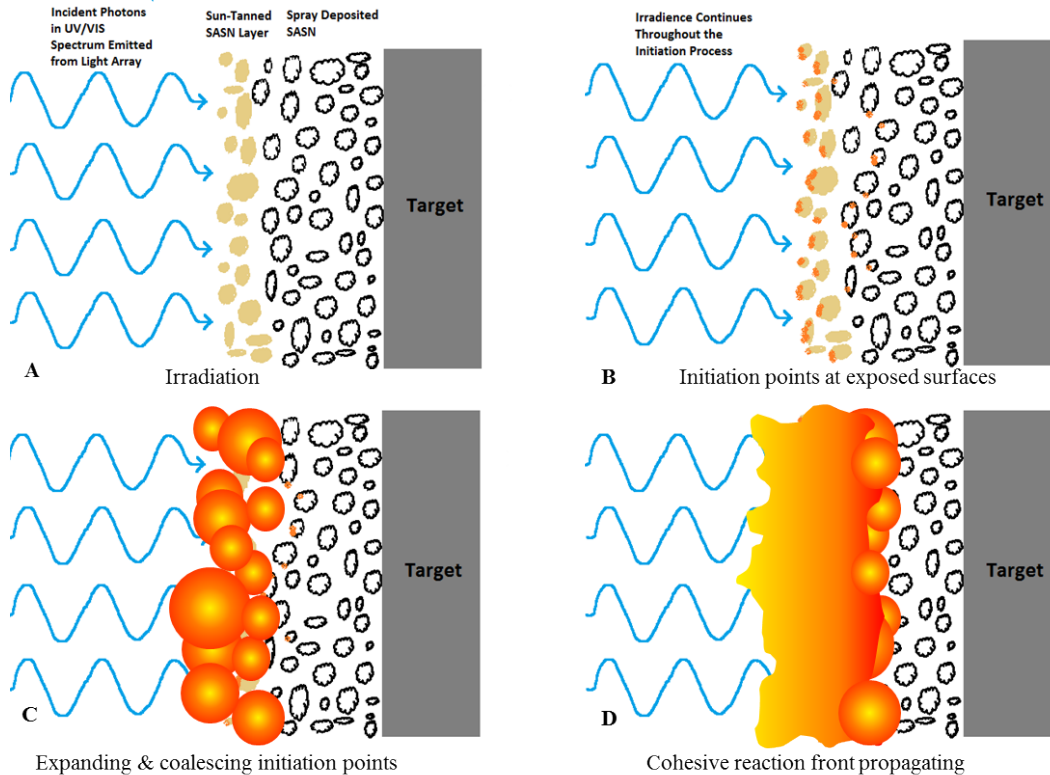


Figure 2-5, Illustration A shows the unreacted porous LIHE subjected to irradiation with subsequent initiation points in illustration B after some induction time. Illustration C is some time after illustration B in which the original initiation points expand in a spherical fashion towards one another to coalesce, leaving reaction products in the centers. The extent of reaction is represented by the color, with red being less reacted and progressing to yellow being fully reacted. Much of the coalescing is done in a regressive fashion. Illustration D shows a cohesive reaction wave that is composed of wavelets that vary spatially at any given time, usually dampening to a quasi-planar wave front.

The TOA timing resolution achieved with the EFOS diagnostic on SASN explosive exceeded any data previously recorded for SASN using other diagnostics [6]. Besides resolving TOA data, the probes produce apparent particle velocity traces similar to other one-dimensional laser interferometer particle velocity measurements with spectral surfaces coated on windowed optical materials. The apparent particle velocity time history produces waveforms that help find

the transient detonation effects of the explosive mix under investigation. The three-dimensional effects of converging shocks/detonation waves, rarefactions, explosive jetting, and the shock-induced change of the index of refraction must be considered and quantified in order to produce actual particle velocity and pressure time histories from EFOS. The experimental configuration that includes the geometry and dimensions of the fibers in a rosette and the explosive coating will need to be defined for appropriate model validation. In addition to these corrections to transform the data into another desirable dataset, the singularity of the transformed data needs to be explored. In other words, the apparent particle velocity time histories may have several combinations of shock and optical effects that result in the same transformed data.

The LIHE team has measured tenths of a kilobar with SASN in contact with fused silica windows with PDV and another well-known laser interferometer, velocity interferometry for any reflector (VISAR) [6]. This pressure range may be close to the lower limit for fused silica fiber optics. However, different applications may need to utilize different optical materials such as polymethyl methacrylate (PMMA) for lower pressure regimes because fused silica is not as sensitive to relatively low pressures. The fused silica fibers allowed measurement of deflagrations and detonations in SASN based explosives in the range of 0.1 to 3 kbars as compared to and indicated by other experimental techniques. Specifically, the LIHE facility has measured pressures in the range of tens of bars with PMMA optical windows and the PDV system. This may be indicative of one potential lower pressure range of a properly designed and calibrated EFOS system. The upper range is likely around the tensile strength of the fiber material on a time scale that allows sufficiently strong rarefactions to enter the fiber material and fracture it, severing the optical path. A caveat at the upper range is that the read time for the apparent particle velocity will be shorter and shorter as the stress level increases. This will likely mean that EFOS will become less of a waveform indicator and more of a TOAD in this upper regime of pressure.

3. EFOS EXPERIMENTAL MEASUREMENTS

A special reduction program developed by Sandia National Laboratories called Sandia Infrared Heterodyne Analysis Program (SIHREN) was used to reduce that raw PDV data [12]. Figure 10 through Figure 17 below document the characteristics of each explosive tested from two separate test series that involved EFOS. The SIHREN program reduced apparent particle velocities are in Figure 3-1 through Figure 3-3, and Figure 3-5 through Figure 3-7. Figure 3-4 and Figure 3-8 are distance-time (XT) plots of the apparent particle velocity half max TOA values for each reducible EFOS probe embedded in the explosive and the relative location from the explosive/air surface. There is a delay in each explosive for the ignition time, which is defined as the first EFOS probe to detect the deflagration wave. The light array emits photons at approximately 5 to 8 μs and the induction time (time from first energy deposition to explosive ignition) is approximately 10 to 15 μs for pure SASN and nominal bulk density 5% m/m Viton B600/SASN and 20 μs for the higher bulk density 5% m/m Viton B600/SASN as measured with EFOS.

The slopes of the lines fitted for the XT plots are the reported reaction wave velocities for SASN, 4% m/m Triton X-100 treated SASN, and 5% m/m Viton B600/SASN. The average reaction front velocity is 0.3 mm/ μs for the pure SASN and that of the Triton treated SASN. The average reaction front velocity for the nominal bulk density Viton B600 doped SASN is 0.1 mm/ μs . The measured velocity did not match the historical detonation velocity as was expected. Therefore, full steady-state detonation of SASN is most likely not achieved for the thicknesses of SASN in this study. Additionally, the reaction front velocity cannot be determined to be a detonation velocity or deflagration velocity without knowledge of the local speed of sound in SASN. However, since SASN is composed of ~90% air, the speed of sound is likely close to that of air, ~0.34 mm/ μs , for this extremely porous explosive. As mentioned in section 2.2, the planarity of the wave should be considered for these velocity measurements.

The measured fiber tip apparent particle velocity time history is indicative of the deflagration/detonation-induced shock strength, rarefaction effects, and the shock-induced change in the index of refraction. The particle velocity trace continues as the combustion products are still under pressure and expand, but the apparent particle velocity changes as a reflected shock from the surface sweeps back up the fiber. As the reflected shock propagates through expanding and probably still chemically condensing combustion products, a second particle velocity jump is induced as seen in Figure 3-1 through Figure 3-3. The reflected shock increases pressure at the interfaces between the fiber and target surface and changes the index of refraction noticeably once again resulting in a change to the apparent particle velocity.

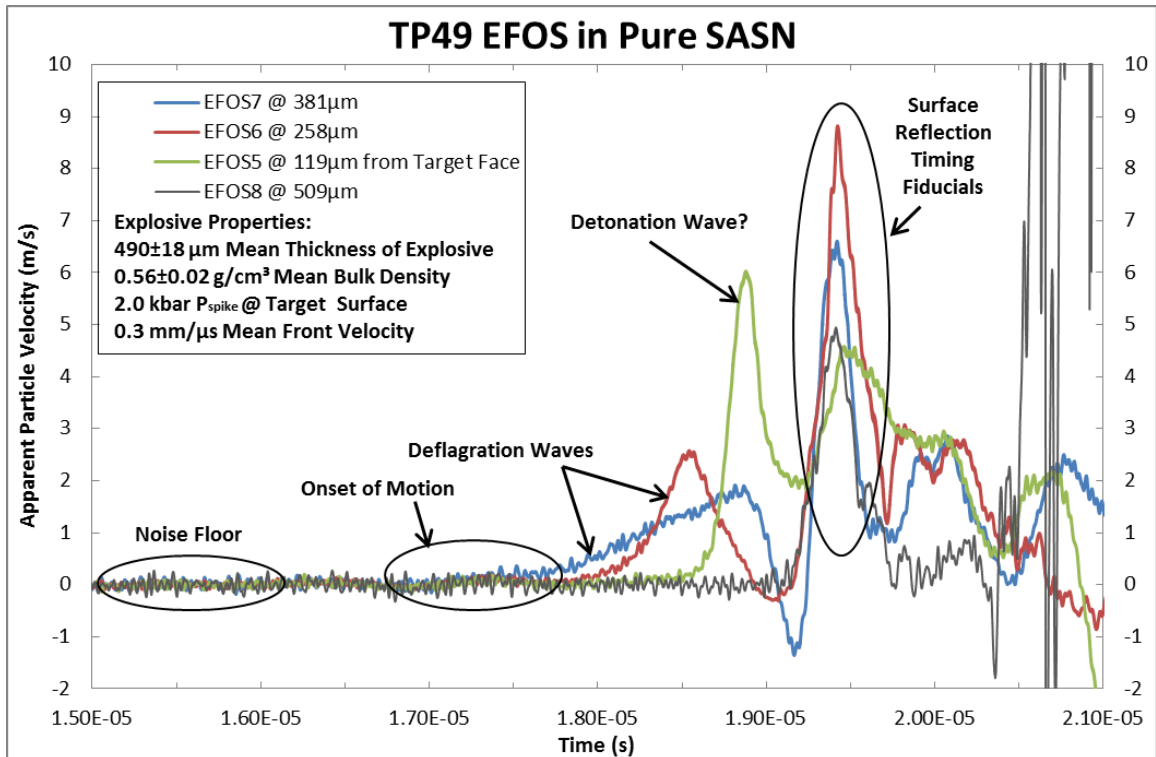


Figure 3-1^[6], Apparent particle velocity traces from EFOS in the unaltered SASN explosive assumed to be ignited from the exposed outer surface by high intensity visible and ultraviolet light.

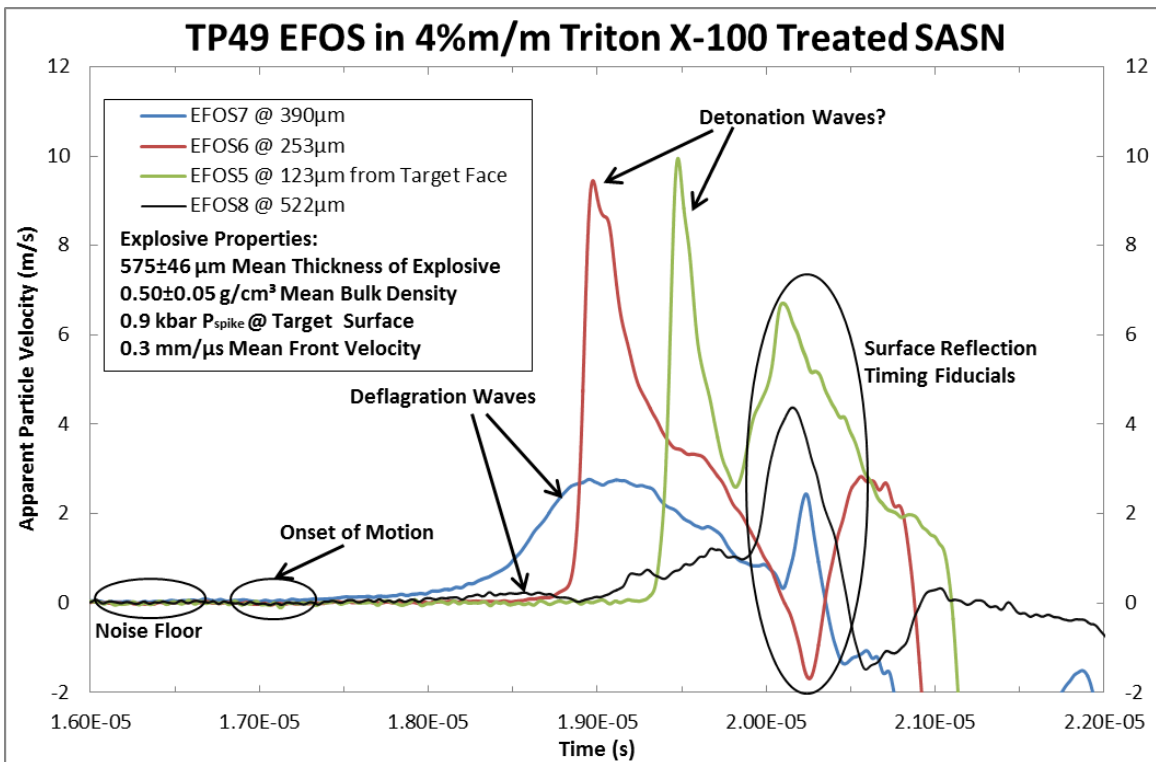


Figure 3-2^[6], Apparent particle velocity traces from EFOS in the 4% Triton X-100/SASN explosive ignited from the exposed outer surface by high intensity visible and ultraviolet light. Notice the PDV6 trace has a negative particle velocity for the suspected surface reflection timing fiducial.

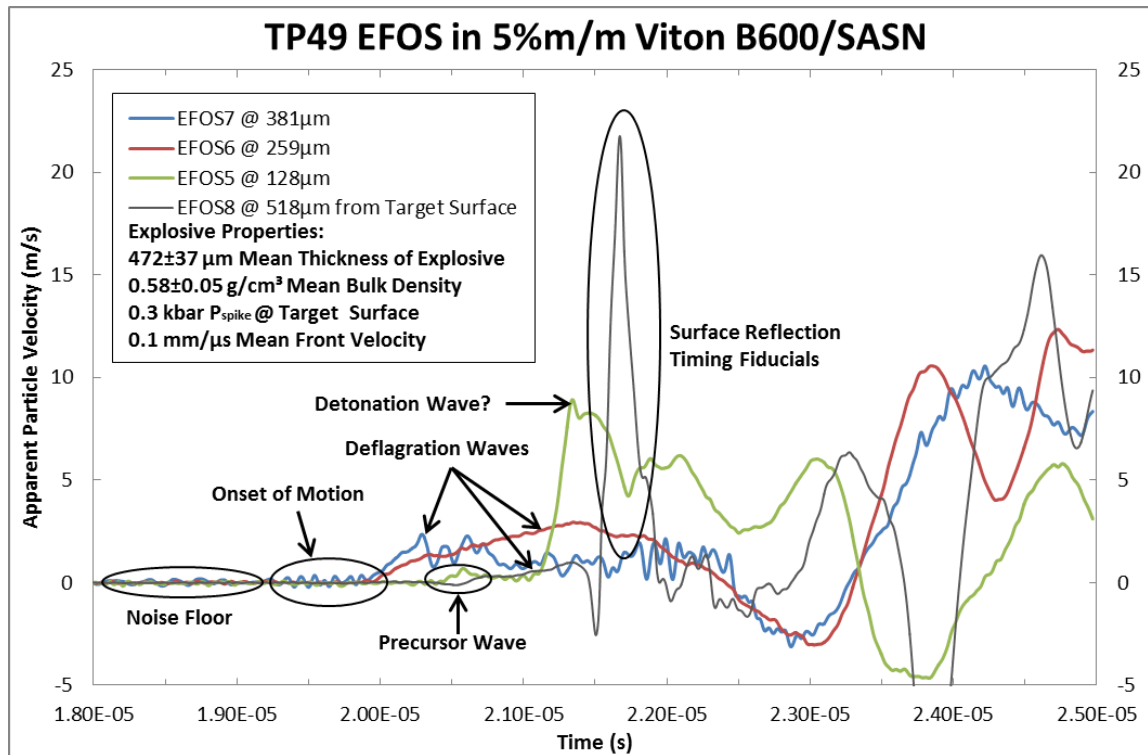


Figure 3-3^[6], Apparent particle velocity traces from EFOS in the 5% Viton B600/SASN explosive ignited from the exposed outer surface by high intensity visible and ultraviolet light. Notice traces PDV 7 (green) and PDV6 (tan) are missing the distinguishable and suspected surface reflection timing fiducials. Notice the inverted suspected surface reflection timing fiducial for the trace of EFO5 (red).

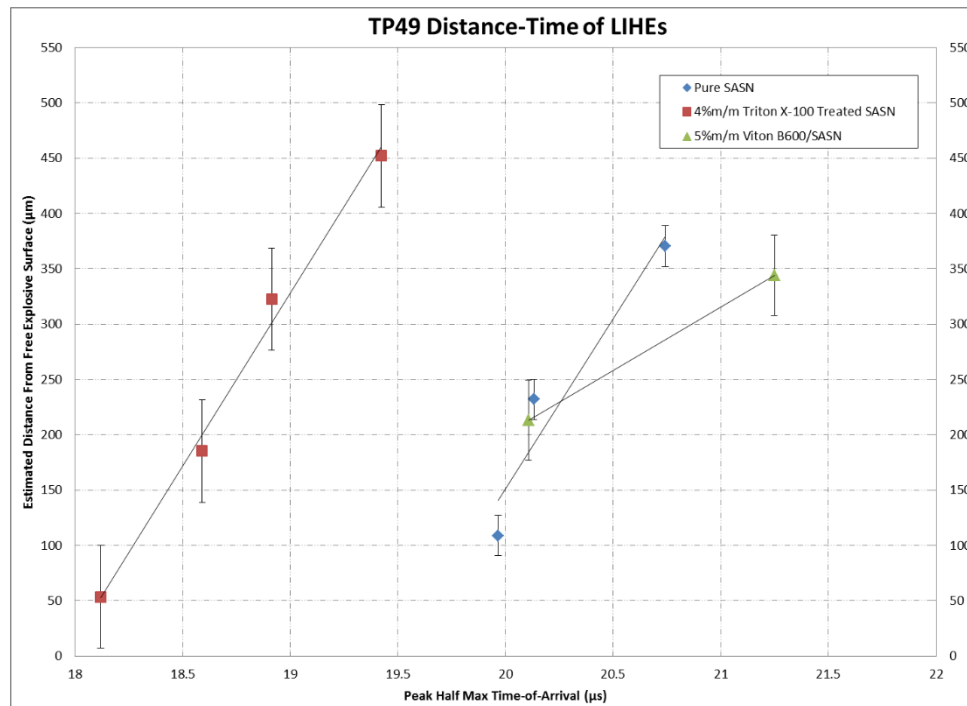


Figure 3-4^[6], XT plot for the EFOS from each explosive mix tested in TP49 giving the first true reaction wave velocities through the thickness of thin spray-deposited explosive when the exposed outer surface is light initiated. The slope of each line is the average wave front velocity for that particular explosive. The wave front velocity is most likely a deflagration velocity. Error bars are deduced from the adjacent coupon thickness measurements.

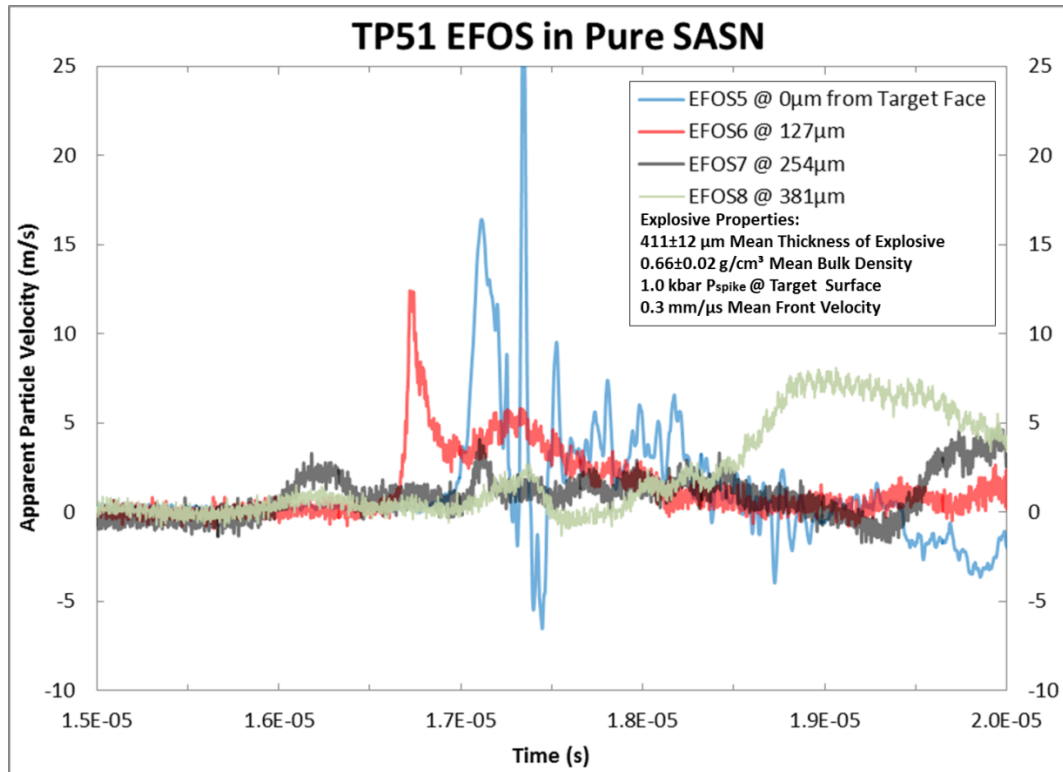


Figure 3-5, Apparent particle velocity traces from EFOS in the pure SASN. The surface reflect shock timing fiducial arrives after the wave front of EFOS5, but smaller amplitude fiducials also appear in the other traces around the same time.

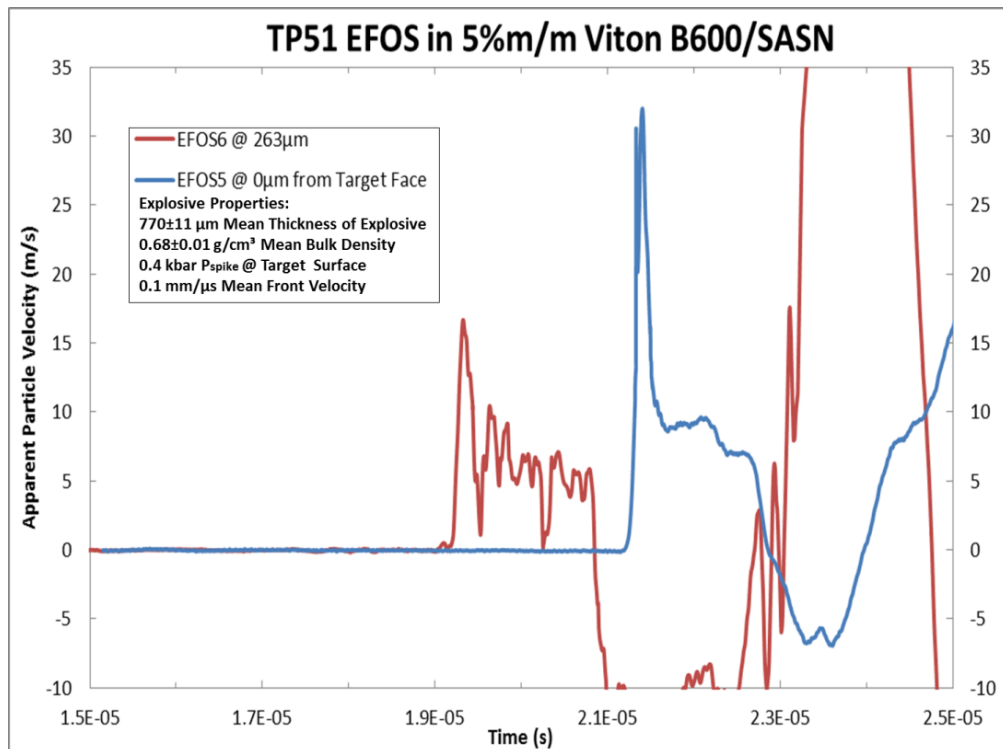


Figure 3-6, Apparent particle velocity waveforms from EFOS in Viton B600 doped SASN explosive. These traces were exceptionally noise-less and gave clear timing for determination of the reaction front velocity. The large amplitude reflected shock timing fiducial appears in the apparent particle velocity trace, EFOS6.

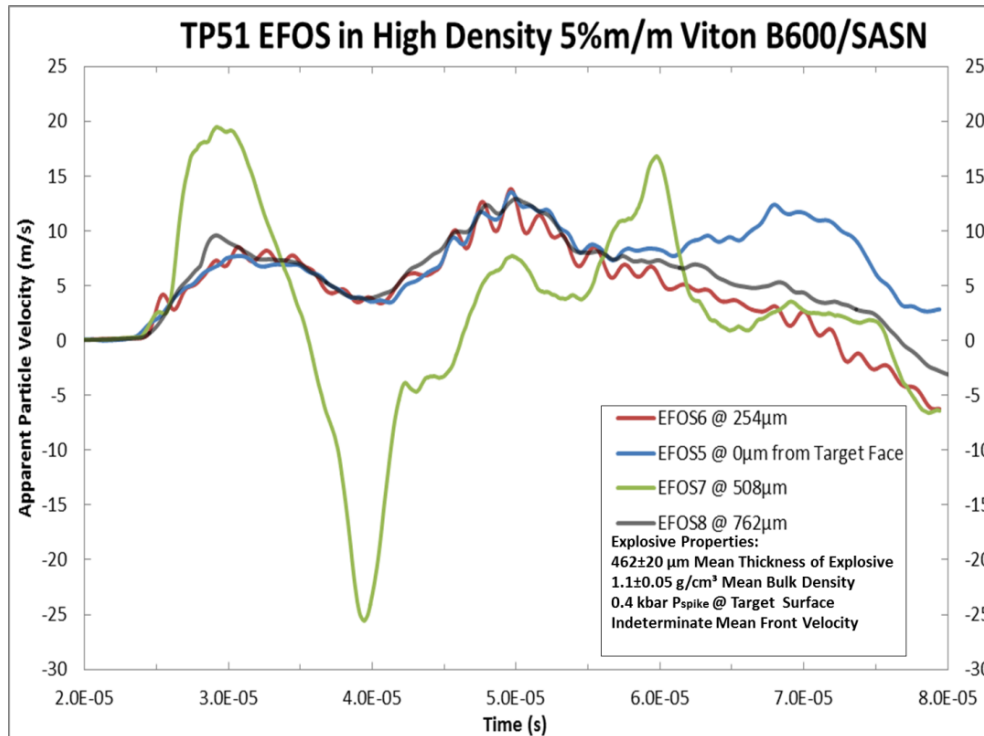


Figure 3-7, Apparent particle velocity time histories for the high bulk density Viton doped SASN explosive. The ignition delay was longer and the traces all nearly overlap for the first 35 μs, except EFOS7. The Viton doped SASN had the tendency to cover the fibers even though they were above the average thickness of the explosive, thus recording similar apparent particle velocity traces. This is an indication of the fiber diameters obstructing the measurement. Video of the explosive during spray deposition showed the protrusion of the fibers under the explosive surface, much like snow covering rocks.

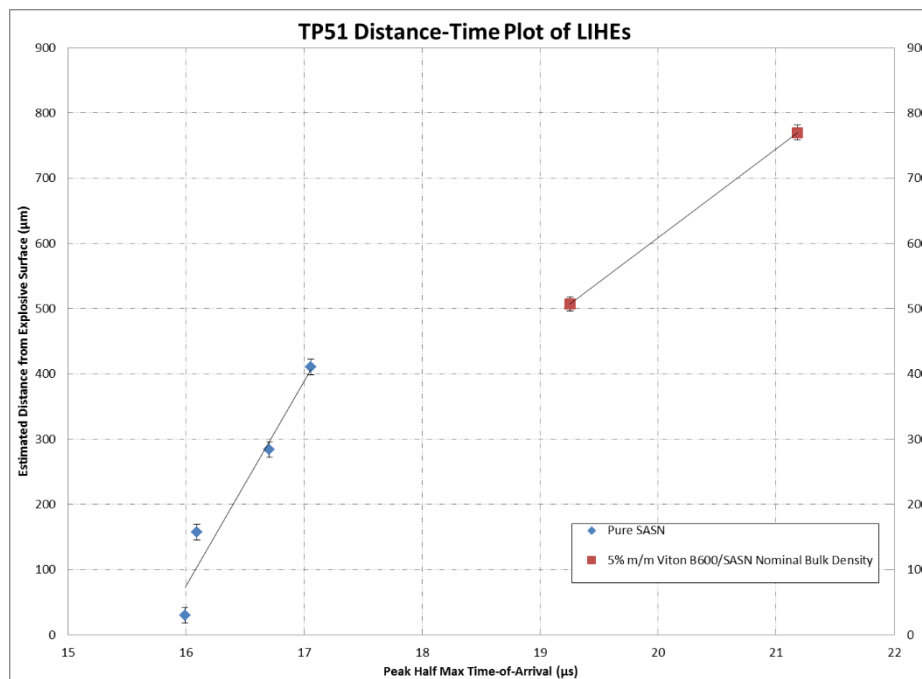


Figure 3-8, XT diagram of the EFOS from two explosive mixes tested in TP51 allowing for reaction wave velocity determination through the thickness of thin spray-deposited explosive when the exposed outer surface is light initiated. The slope of each line is the average wave front velocity for that particular explosive. The wave front velocity is most likely a deflagration velocity. Error bars are deduced from the adjacent coupon thickness measurements.

4. EFOS SIMULATION RESULTS

Techniques to reduce the data into quantitative transient detonation behavior are in development. The diagnostic in the aforementioned experimental configuration had a helpful timing fiducial for each probe that allowed each probe to be a stand-alone TOA diagnostic. This was mentioned earlier as a, “reflected shock timing fiducial.” The special timing fiducial was confirmed by CTH hydrocode analysis with a simple two-dimensional configuration of arbitrary SASN modeled with the Jones-Wilkins-Lee approximation, two EFOS, and a drilled-out aluminum substrate. This model simulated some of the typical geometries seen in experiments with EFOS. The explosive model did not account for transient detonation phenomena. A model for the transient phenomena will be built based on the data collected from EFOS and other explosive output diagnostics. Figure 4-1 through Figure 4-3 below show the results from the model and the ability of the model to give an explanation of the second particle velocity jump that is seen in some instances. All the apparent particle velocity traces, except possibly Figure 3-7, display the special timing fiducial as well as the waveform of the explosive. However, there are some unexplained inverted surface reflection timing fiducials seen in Figure 3-2, Figure 3-3, Figure 3-6, and potentially Figure 3-7.

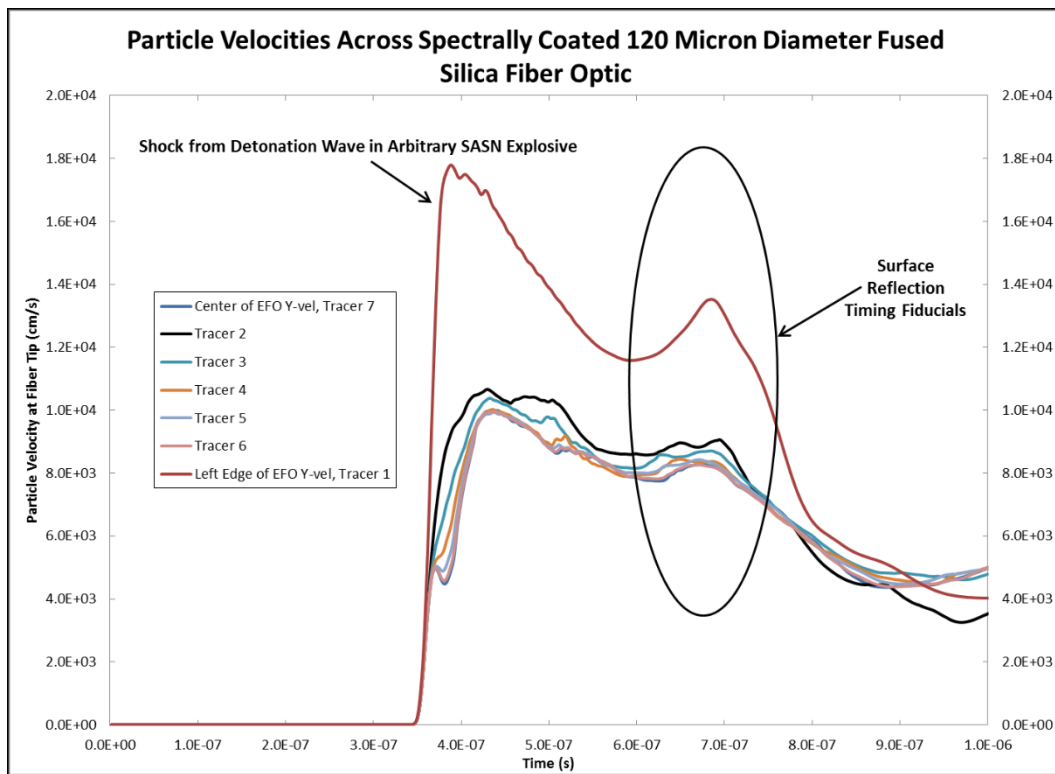


Figure 4-1^[6], Two-dimensional CTH modeling results for arbitrary SASN detonation wave impacting one EFOS tip and reflecting off the aluminum substrate. This is the particle velocity in the fiber that the EFOS would see if corrected for the index of refraction as well as the shock-induced change in the index of refraction. However, rarefaction effects are still evident and need to be corrected for in order to produce the true particle velocity of the fiber tip.

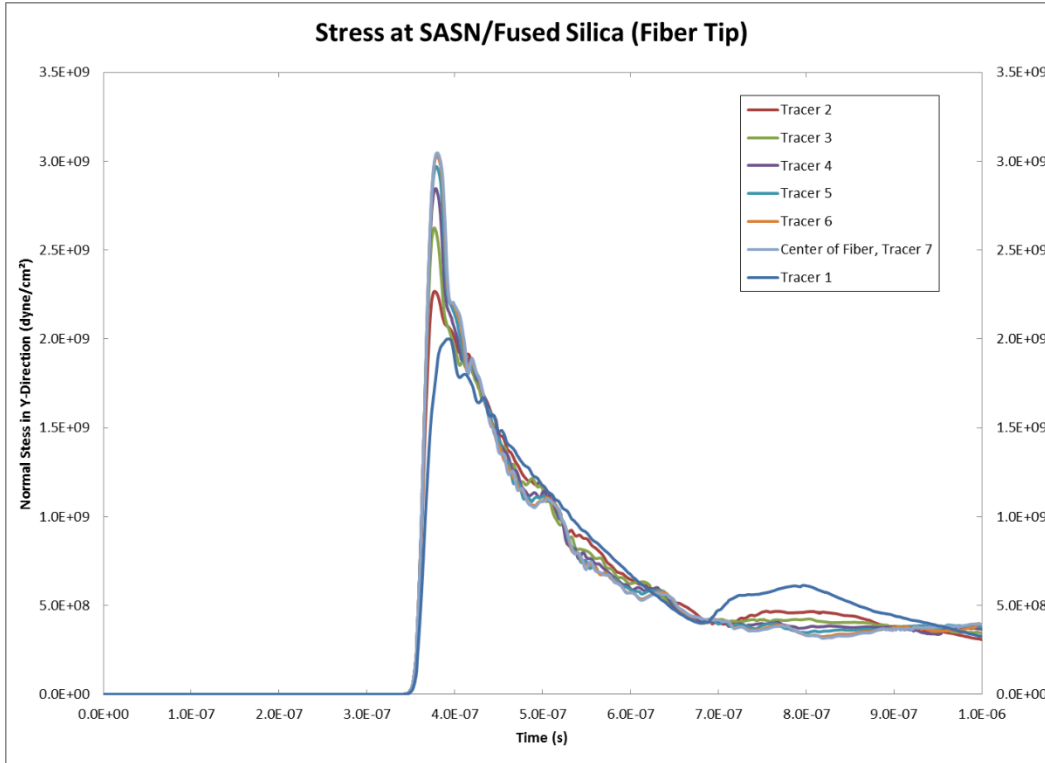


Figure 4-2, Stress time history corresponding to the same tracer locations from Figure 17 above. The second major particle velocity jump has a complementary stress. This reflected stress emanated from an input stress that is the deflagration/detonation wave. Thus, through proper transformations, the EFOS could reveal the pressure time history of an energetic material at that location in the flow.

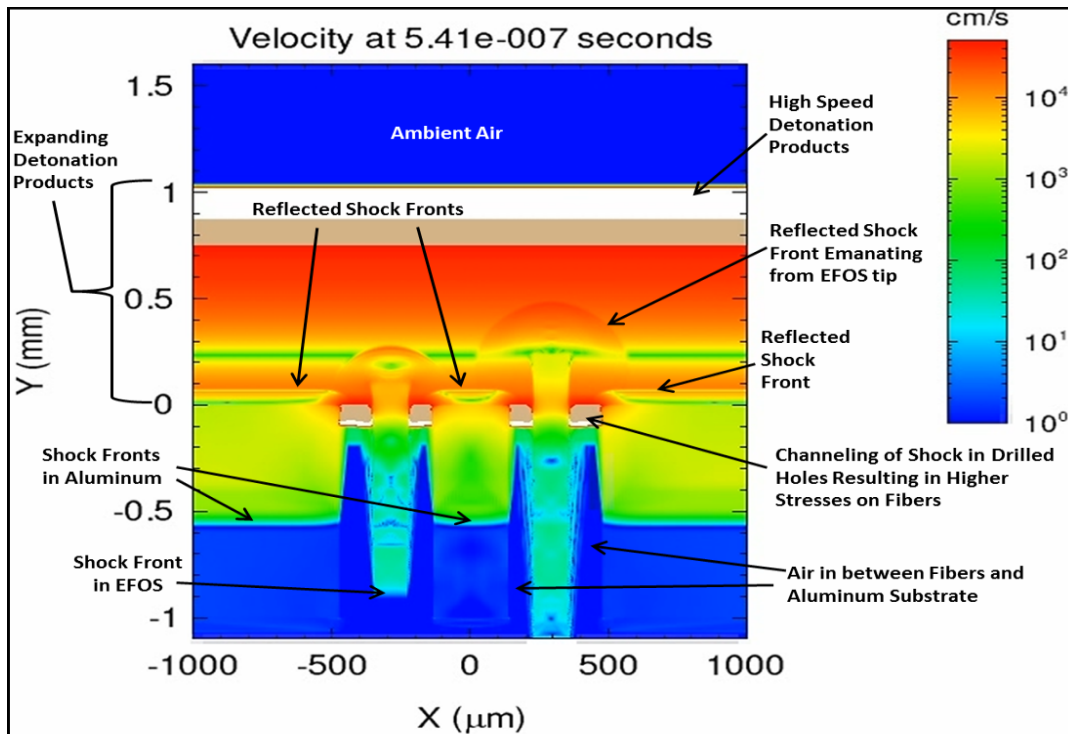


Figure 4-3^[6], Image from two-dimensional CTH simulation of two EFOS in a typical experimental geometry seen in TP49. The tallest EFOS is at an elevation of 254 μm and the shorter one is at 127 μm . The white and gray colored areas in the model are particle velocities that are above the upper color map range.

5. CONCLUSION

Embedded Fiber Optic Sensors coupled to a photonic Doppler velocimetry system are novel devices used for novel applications in research of transient detonation and shock wave phenomena. However, the device is not limited to pure detonation and shock wave studies, but can measure reactive and inert dynamic pressure pulses of the non-shock nature. Others have developed microscale devices based on similar principles, but for different applications and modes of detection. Also, the other comparable microscale devices have not incorporated numerous probes at different locations within the material of interest. This multi-probe approach saves valuable time, effort, and materials for an experimentalist since the probes are relatively inexpensive.

The fiber material, spectral coating, experimental arrangement, and detection system can be changed to accommodate the needs of the researcher for different pressure regimes, robustness of the diagnostic in harsh environments, and to minimally perturb the medium under investigation. This study pushed this technology to measure data that was unattainable without microscopic sensors and give the authors unprecedented insight into the transient nature of silver acetylide-silver nitrate explosive. Historical detonation velocity data proved to be insufficient to represent the reaction wave front velocity of SASN and was twice to four times faster than what was measured with EFOS. The minimally invasive nature of the probes in this study gave repeatable reaction front velocity measurements for pure SASN and nominal bulk density Viton B600 doped SASN. However, the higher bulk density Viton B600 doped SASN did show visual evidence of the probes causing explosive to build up on and around the fiber tips creating a protrusion of explosive in the area. This last case was the only one to have an indeterminate reaction front velocity and the invasiveness of the probes may be to blame. Although the probes in this last case were invasive to the measurement, the possibility exists that the higher bulk density caused a change in the time and distance it takes for the reactive wave front to become cohesive.

These probes were able to produce waveforms similar to those captured with other diagnostics that measure pressure, giving credence to EFOS being capable to generate a transformed version of the particle velocity and pressure. In many of the pure SASN traces as well as the Triton X-100 doped SASN; there is a clear trend of apparent particle velocity growth as a function of distance and time. Again, this was captured in other diagnostics not presented in this study, but with EFOS it is apparent. The DDT and BUD behavior of SASN can be measured in a single experiment. Of course, this requires knowledge of when DDT occurs in terms of the velocity of the reaction front, but the waveforms generated aid in determining this qualitatively.

The type of data collected by EFOS is extremely important to understand and develop models for the explosive behavior of LIHEs, other explosives, and the shock/non-shock nature of inert materials. Hydrocode simulation of the experimental configuration presented here provided insight into interpretation of the data. There is now a need for precise profilometry of the probes and the explosive spray coating to provide the model with a closer match to the experimental configuration. The CTH modeling exercise fell short in determining the apparent particle velocity as the EFOS diagnostic would see it because a laser interferometer function is not built into the program.

6. REFERENCES

1. Barker, L.M., Hollenbach, R.E., *Shock-Wave Studies of PMMA, Fused Silica, and Sapphire*, Journal of Applied Physics, Volume 41, Number 10, September 1970.
2. Benham, R.A., *An Initiation and Gas Expansion Model for the Light-Initiated Explosive Silver Acetylide-Silver Nitrate*. Albuquerque, NM: Sandia National Laboratories, February 1980. SAND79-1829.
3. Wilden, M.W., *Investigations Pertinent to Ignition of Sprayed Layers of Silver Acetylide-Silver Nitrate*. Albuquerque, NM: Sandia National Laboratories, May 1986. SAND85-1859.
4. Baker, W.E., Hoese, F.O., Silverman, S., *Development of Capabilities of a Light-Initiated, Sprayed Explosive*. San Antonio, TX: Southwest Research Institute, September 1969. Technical Report IR Project No. 02-9008-08.
5. Johnson, R., *Final Report on SASN Investigation*. Phoenix, AZ: Unidynamics, February 26, 1987. Sandia Contract No. 04-1414, Document No. MCD-123.
6. Chavez, M.A., Covert, T.T., *Synthesis, Microstructure, and Explosive Properties of Spray-Deposited Silver Acetylide-Silver Nitrate Composite Light Initiated High Explosives*. Albuquerque, NM : Sandia National Laboratories, April 2013. SAND2013-3088C. Presented at the 83rd Shock & Vibration Exchange (SAVE) Symposium.
7. Dolan, D.H., *Foundations of VISAR Analysis*. Albuquerque, NM : Sandia National Laboratories, April 2006. SAND2006-1950.
8. Jensen, B.J., Holtkamp, D.B., Rigg, P.A., Dolan, D.H., *Accuracy Limits and Window Corrections for Photon Doppler Velocimetry*, Journal of Applied Physics, Volume 101, 2007.
9. Strand, O.T., Goosman, D.R., Martinez, C., Whitworth, T.L., Kuhlow, W.W., *A Novel System for High-Speed Velocimetry Using Heterodyne Techniques*. Livermore, CA: Lawrence Livermore National Laboratories, November 2005. UCRL-JRNL-216919.
10. Willis, M.W., *Personal Communication*. Sandia National Laboratories, September 2010.
11. Willis, M.W., *LIHE Data Instrumentation Pre-Shot Notes for TP2012_48 Explosive Characterization and Development. Revision 5*. Albuquerque, NM: Sandia National Laboratories, March 2012. Memorandum.
12. Ao, T. and Dolan, D. H., *SIRHEN: a Data Reduction Program for Photonic Doppler Velocimetry Measurements*, SAND2010-3628, Sandia National Laboratories, Albuquerque, NM, June 2010.

